23rd Australasian Fluid Mechanics Conference – 23AFMC
Sydney, Australia
4-8 December 2022
Paper No: AFMC2022-020

Particle Image Velocimetry Investigations on the Flow Structure of Buoyancy Vortices

Z. WANG [1]*, N. A. Hawkes [1], M. MacDonald [1], J. E. Cater [2] and R. G. J. Flay [1]

[1] Department of Mechanical and Mechatronics Engineering,

The University of Auckland, Auckland 1010, New Zealand

[2] Department of Engineering Science,

The University of Auckland, Auckland 1010, New Zealand

* Email: zwan472@aucklanduni.ac.nz

Abstract

Measurements were conducted within the flow field of a buoyancy-driven vortex at laboratory scale with a constant input heat flux. Time-averaged velocity data was obtained using two-dimensional Particle Image Velocimetry (PIV). The velocity profiles in both cross-sectional and vertical planes were measured at heights of 0.3 m, 0.45 m, and 0.6 m above the ground level, and the tangential, radial and vertical velocity components were measured. Detailed flow characteristics have been investigated, including flow patterns and axial vorticity for both the inner and outer core regions. The local swirl ratios around the core are also calculated, ranging from 1.17 to 1.45, indicating a two-cell vortex structure was found at all three elevations.

1. Introduction

Buoyancy vortices, such as dust devils and waterspouts, are buoyancy-driven and self-sustained columnar flows that commonly appear in the atmosphere. These vortices develop due to hot plumes in deserts or warm sea surfaces, with a wide range of scales from a few metres to several kilometres in height. The heated surface provides a source of buoyancy so that air parcels rise. Loose dust on surfaces or condensation of moisture can make the vortex structure visible (Hess & Spillane, 1990; Rennó et al., 1998; Renno, 2004). Field measurements show that dust devils can have maximum mean tangential velocities of around 10 m/s near the ground (Fitzjarrald, 1973; Sinclair, 1973). For waterspouts, measurements show higher mean tangential velocities with a peak value of 80 m/s (Golden, 1974a, 1974b).

Field measurements of natural vortices have been complicated by transient ambient conditions and have been limited to narrow height ranges. In addition, the accuracy of measurements of natural vortices are limited when interpretated from images and videos, as the flow field of vortices only becomes visible from either condensation of the droplets or from dust particles, which may not follow the flow accurately (Lugt, 1989). Therefore, laboratory studies on buoyancy vortices in a controlled environment are required to elucidate the entire flow structure.

A number of laboratory investigations have been carried out on buoyancy vortices. Early measurements were restricted by the techniques and instrumentation available at that time. One of the earliest laboratory buoyancy vortex studies was by Mullen and Maxworthy (1977), where the flow was visualised and measured using helium-filled soap bubbles. However, the accuracy of the measurements and the flow visualisation near the vortex core were limited due to the short survival time of the bubbles, and the limitation of the recording system. Therefore, the primary objectives of this research are to conduct preliminary investigations to characterise the time-averaged flow near the core, the potential flows in the outer region, and the vortex structure in detail by using Particle Image Velocimetry (PIV).

2. Methodology

2.1 Experimental Apparatus

An experimental apparatus was designed and built by Hawkes et al. (2020), named the 'Buoyancy Vortex Extension Cabinet', as shown in Figure 1(a). The vortex cabinet has an overall height of 6 m, and a crossflow extractor is mounted at the top to provide a neutral stratification condition within the cabinet to prevent the accumulation of the warm air. The air enters the apparatus through vertical ducts to prevent any disruption from other laboratory activities. The source of buoyancy is provided by an aluminium hot plate, which provides controlled heat input with a heating area 0.7 m in diameter. A controller is used to adjust the heating power of the hot plate. The source of swirl is given by 12 stationary swirl vanes (0.15 m wide, 0.3 m tall) evenly distributed around the hot plate. The vanes are fixed in position but are free to pivot along their central axis, allowing adjustable vane angles as different input conditions. The vane angles can be set at 30°, 45°, 60° and 75° relative to the radial direction. In this study, the hot plate power was set to be 2.5 kW with the vane angles set at 60° to the radial direction, as it subjects to a large swirl of input, which tends to show a two-cell vortex structure according to early experimental study by Mullen and Maxworthy (1977). The configuration of the main components inside the rig is shown in Figure 1(b).

Figure 1. Images of the experimental configuration showing (a) the external view of the Vortex Cabinet, (b) the main components inside the rig.

2.2 PIV Setup

The flow field was illuminated by a 5 W continuous-wave Nd: YAG laser with a wavelength of 532 nm. A Powell lens with 15° fan angle was used to shape the beam into a uniform thickness (3~5 mm) light sheet across the flow field of interest. Tracer particles were produced by dripping a solution of propylene glycol, glycerine and water mixture onto centre of the hot plate, which form micron-sized droplets when heated. Schematic diagrams of the PIV configurations for the cross-sectional and vertical plane measurements are shown in Figure 2.

A high-speed monochrome CMOS camera (FLIR Blackfly S) was used to capture images continuously at an acquisition rate of 430 Hz, with a resolution of 720 × 540 pixels in the cross-sectional and vertical directions. Nikon f = 50 mm, f # 1.8, and f = 28 mm, f # 2.8 lenses were used for the cross-sectional (r, θ) and vertical (meridional) (x, z) plane measurements, respectively. A calibration object with a two-dimensional uniform grid was used for camera calibration prior to every measurement. The field of view (FOV) and other key parameters are summarised in Table 1, and the height for the vertical plane measurement refers to the height of the midpoint of the FOV.

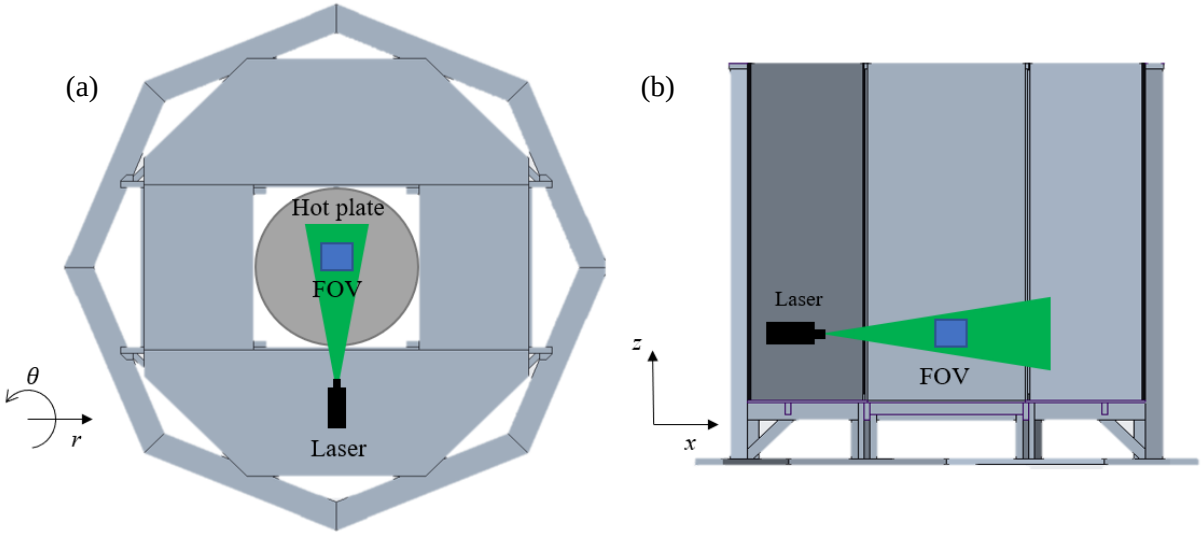

Figure 2. Schematic diagrams showing the PIV arrangements for (a) cross-sectional plane measurements, and (b) the vertical plane measurements.

Measurement Plane	FOV [mm×mm]	Height z [m]	Spatial Resolution [pixels/mm]
Cross-sectional (r-θ)	133×100	0.60	5.41
	148×111	0.45	4.86
	162×122	0.30	4.44
Vertical (x-z)	174×130	0.60	4.14
		0.45	
		0.30	

Table 1. PIV measurement parameters for cross-sectional and vertical Plane

2.3 Data Acquisition and Processing

The images were recorded and stored in the camera buffer and transferred directly to computer through a USB 3.1 cable, and time-averaged images of the flow field were obtained. The time-averaged analysis included a long sequence with 1800 frames acquired from different time periods (approximately 0.7 seconds, 300 frames with 6 minutes gap between each period) for over 30 minutes duration in total. The images were processed using PIVlab (Version 2.56) in MATLAB (Version R2020b). The time-resolved image pairs were pre-processed by applying the contrast limited adaptative histogram equalisation, with a window size of 64 pixels. The image pairs were then analysed by using a multi-pass FFT algorithm, with an initial interrogation area of 128 × 128 pixels for the first pass, 64 × 64 pixels for the second pass and narrowed down to a final pass of 32 × 32 pixels with 50% overlapping. The post-processing applied a standard deviation filter with a threshold of 3σ on the velocity vectors and a local median threshold filter of 3×3 vectors to eliminate spurious vectors.

Velocity components and their positions were converted from x-y Cartesian coordinates into r-θ cylindrical coordinates, where the tangential (Vt) and radial (Vr) velocity components were derived from the cross-sectional (r, θ) plane measurements and the vertical (Vz) velocity component was obtained from the vertical (x, z) plane measurements. The centre of the vortex was identified as the

position where the velocity magnitudes were at the lowest. The radius of the vortex core (r_c) was defined as the distance from the centre to where the maximum tangential velocity $V_{t,max}$ occurred. The velocity profiles and core radii are normalised by the maximum tangential velocity $V_{t,max}$ and the core radius r_c at height z = 0.6 m. To quantify the tangential flow strength and swirl, the axial circulation Γ and Reynolds number (*Re*) were calculated by Eq. (1) and (2) according to Simpson and Glezer (2016) ,

$$\Gamma = \oint_0^{2\pi} V_t r \, d\theta = 2\pi r V_t \tag{1}$$

$$Re = \frac{\Gamma}{2\pi \upsilon} \tag{2}$$

where r is the radius of the vortex and υ is the air kinematic viscosity. The vorticity ω_z in vertical direction was calculated by Eq. (3),

$$\omega_z = \frac{1}{2}\left(\frac{\partial v}{\partial x} - \frac{\partial u}{\partial y}\right) \tag{3}$$

where u, v are the Cartesian velocity components in the cross-sectional plane. In this study, the time and azimuthally averaged axial vorticities were derived, by assuming the azimuthal variation in the time-averaged results is negligible, which is also used by Simpson and Glezer (2016). The swirl ratio S was calculated from the method introduced by Church et al. (1979), quantifying the ratio of the tangential to vertical momentum, as defined in Eq. (4). Q is the vertical volumetric flow rate of the core region, defined by Eq. (5),

$$S = \frac{r\Gamma_{max}}{2Q} = \frac{\pi r_c^2 V_{t,max}}{Q} \tag{4}$$

$$Q = 2\pi r_c \int_0^{r_c} V_z(r)\, dr \tag{5}$$

According to Church et al. (1979), vortex structures are strongly correlated with this parameter. It is suggested that a single-cell vortex structure occurs for $0 < S \lesssim 0.1$, vortex breakdown from a one-cell to a two-cell structure occurs for $0.2 \lesssim S \lesssim 0.3$, and a two-cell vortex occurs for $S > 0.4$ (Bischof et al., 2020).

3. Results and Discussion

3.1 Cross-sectional Plane Measurements

The cross-sectional time-averaged PIV results are shown in Figure 3. The velocity magnitude (Figure 3a) shows the vortex structure has the largest in-plane velocity magnitude at z = 0.3 m and the lowest at z = 0.6 m, and core sizes also differs with the change in heights.

The azimuthally-averaged velocities were calculated with an incremental step size of 2 mm along the radius from the vortex centre to the furthest point in the measurement plane to eliminate the asymmetry effect that would cause biased results. The normalised azimuthally and time-averaged radial and tangential velocity profiles are shown in Figure 3(b). The results suggest that the tangential velocity profiles have similar trends to a Rankine vortex model, regardless of change in elevation. The tangential velocities increase linearly along the radius within the inner core region for $r/r_c < 0.7$, suggesting that the inner structure behaves like solid-body rotation. They peak at $1 < r/r_c < 1.5$, where the edges of the vortex cores are located. For $0 < r/r_c < 1.7$, the radial velocity components (V_r) have positive values, indicating radial outward flows, with the magnitudes much smaller than the tangential components (V_t). The radial components reach zero at around $r/r_c > 1.7$ and change to radial inwards flow, implying radial entrainment of the surrounding air is occurring.

For the lower part of the structure at z = 0.3 m, the core diameter is the largest at r/r_c = 1.40, where the tangential velocity is $V_t/V_{t,\,max}$ = 1.16. For the middle part of the structure at z = 0.45 m, the core diameter and tangential velocity decrease, with $V_t/V_{t,\,max}$ = 1.10 at r/r_c = 1.15. Both tangential velocity and core radius appear to be minima at z = 0.6 m, indicating weaker flow strength in the higher part of the structure.

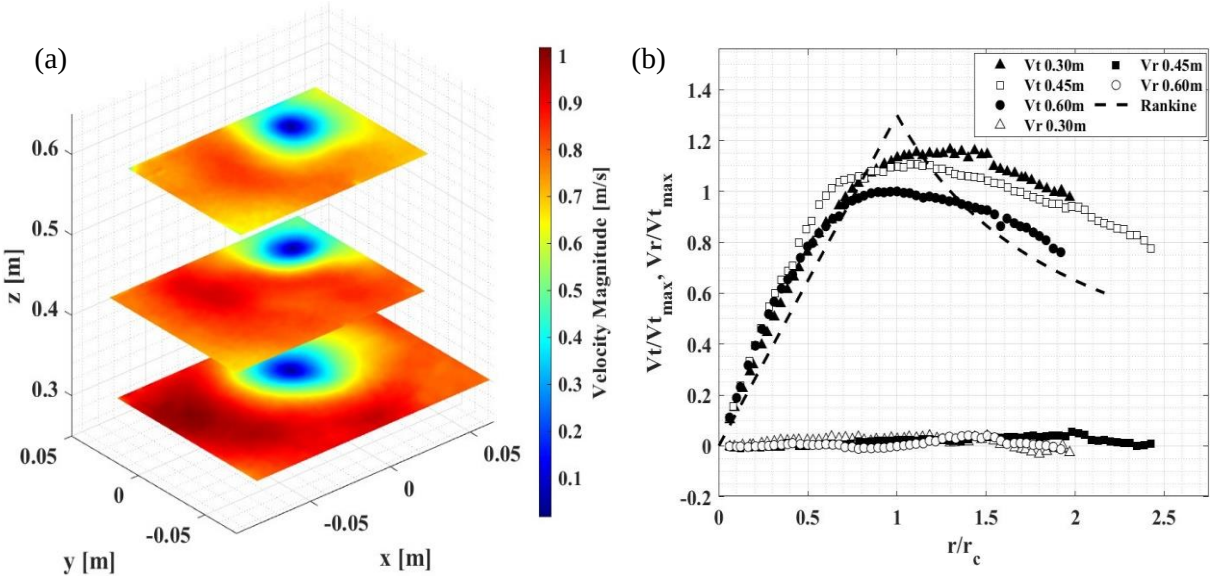

Figure 3. Time-averaged PIV results showing (a) contours of cross-sectional plane velocity magnitude, (b) normalised azimuthal averaged velocity profiles at heights 0.3, 0.45 and 0.6 m above the hot plate.

The tangential velocity profiles measured at lower heights (z = 0.3 m) are compared to the field measurements of the lower structure of waterspouts (Golden, 1974a) and dust devils (Sinclair, 1973) in Figure 4, where V_t^* and r^* are the tangential velocities and radii, normalised by their maximum values. The measurements of waterspouts and dust devils were taken at 15 m Mean Sea Level (MSL) and 9.4 m (31 ft) above the ground, respectively. As shown in Figure 4, the plots show similarity of the tangential velocity profiles from a laboratory generated vortex to the natural vortices regardless of their scale.

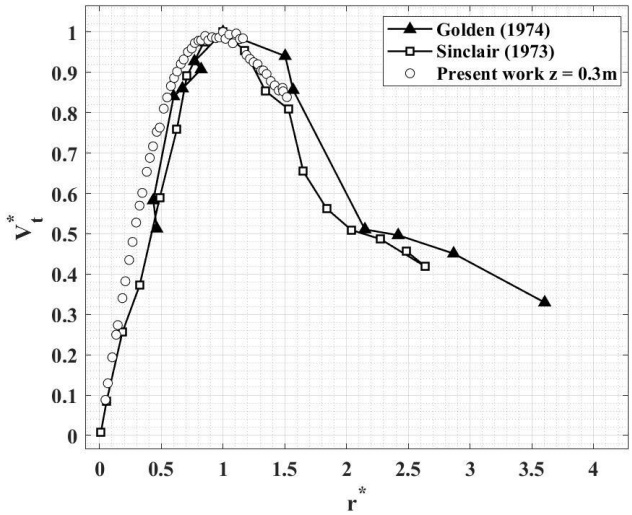

Figure 4. Comparison of the normalised tangential velocity profile of laboratory generated vortex (○), with field measurements of a waterspout (▲) and a dust devil (□) at lower altitude.

The vertical components of vorticity ω_z are shown in Figure 5. The azimuthally and time-averaged vertical vorticity are normalised by the angular velocity of the vortex core (Ω_{z0}), calculated from the maximum tangential velocity and relative core radius at z = 0.6 m. The results in Figure 5(a)

indicate that the strongest vorticities form within the vortex core centre at all heights. In Figure 5(b), the strongest axial vorticities occur near the centre of the core at $r/r_c = 0.2$, and then they decay rapidly along the radius for $0.5 < r/r_c < 1.5$. The vorticities approach zero at $r/r_c > 1.5$, indicating irrotational potential flow in the outer core region. The trends in axial vorticities show good agreement with the experimental results by Simpson and Glezer (2016).

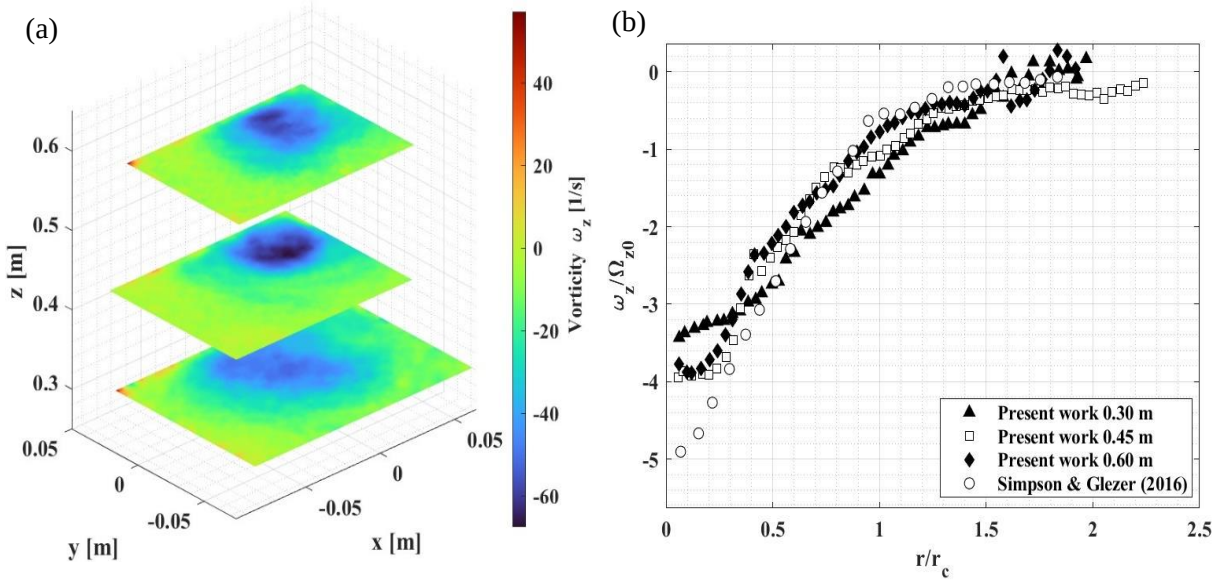

Figure 5. Time-averaged PIV results showing (a) contours of cross-sectional plane vertical vorticity, (b) normalised azimuthal-averaged axial vorticity at heights 0.3, 0.45 and 0.6 m above the hot plate.

3.2 Vertical Plane Measurements

The vertical plane measurements were carried out at the meridional plane of the structure, and the results are normalised by the maximum tangential velocity measured at 0.6 m. Figure 6(a) shows symmetric distributions of the vertical velocity along the radius, and the lowest V_z are found in the core centre ($r/r_c = 0$) across heights from z = 0.25 to 0.65 m above the hot plate. This suggests that upward motion was deaccelerated in the vortex core centre, supported by the instantaneous measurements (not shown), which captured downward flows at the core centre. The magnitude of the descending motion is small, caused by the interaction with the ascending motion outside, resulting in the magnitude of the time-averaged vertical velocity tending toward zero in the centre. This finding is supported by the previous study from Kuo (1966), who suggested similar vertical velocity distributions for two-cell vortex structures.

Figure 6(b) shows that the vertical velocities peak at the vortex core for $1 < r/r_c < 1.5$, corresponding to the locations where the maximum tangential velocities V_t occur. This finding agrees with the field studies on dust devils (Fitzjarrald, 1973; Sinclair, 1973) and the analytical solutions of two-cell type vortices (Kuo, 1966). Then V_z decreases in the outer core region ($r/r_c > 1.5$), corresponding to locations where the axial vorticities ω_z approach zero, indicating irrotational potential flow regions. The maximum vertical velocities are found to be smaller than the tangential velocities, with magnitudes 60 - 70% of the maximum V_t at $z = 0.6$ m.

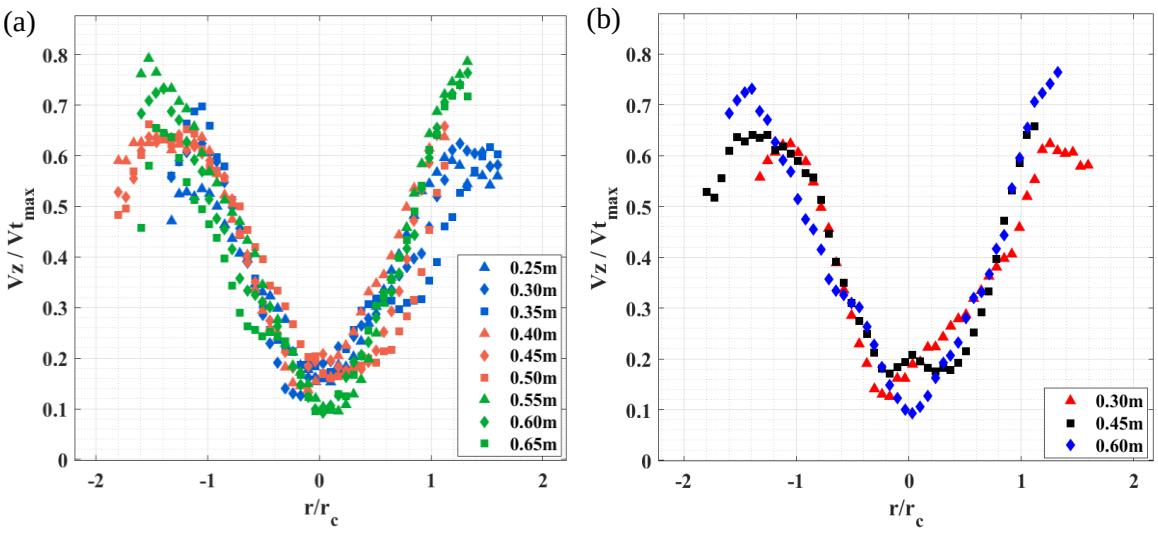

Figure 6. Time-averaged normalised vertical velocity profiles (a) from 0.25 to 0.65 m (b) specific heights of 0.3, 0.45 and 0.6 m above the hot plate.

With vertical and tangential velocity being measured, the local swirl ratios (*S*) and core Reynolds numbers (*Re*) for the vortex structure were calculated within the radius $r/r_c = 1.5$, covering the flows within core regions from all measured heights, and the derived results are summarised in Table 2. The core Reynolds numbers have values around 2000, and they remain almost invariant against height. The results show a good agreement with the experimental study by Simpson and Glezer (2016). This is consistent with the axial vorticity calculated in the previous section (Fig.5), revealing that the vortex core structure remains self-similar within the measured height. The consistency is also shown in the flow rates calculated within the core region ($0 < r/r_c < 1.5$), with an average value of 0.0141. The local swirl ratios, derived from equation (4), have values greater than 1.0, suggesting a two-cell vortex structure with very large swirls (Church et al., 1979). The swirl ratios decrease gradually with the increase of height, as a result of decay in tangential momentum.

Height *z* [m]	Core Reynolds Number	Maximum in-plane V_t [m/s]	Q [m^3/s]	Swirl ratio *S*
0.30	2100	0.91	0.0135	1.45
0.45	2100	0.86	0.0147	1.25
0.60	1900	0.78	0.0142	1.17

Table 2. Parameters derived from PIV results to evaluate the local swirl ratios at $0 < r/r_c < 1.5$.

4. Conclusions

Two-dimensional, time-averaged PIV measurements have been carried out to investigate the flow structure of a laboratory-scale buoyancy vortex created using a heating power of 2.5 kW and swirl vane angles set at 60°. From the cross-sectional measurements, azimuthally-averaged tangential velocity profiles were obtained, showing similar trends to the Rankine vortex model and field measurements of natural vortices at lower heights. The highest in-plane velocity magnitude was found to be in the lower part of the vortex structure, and it decreased with increasing height, as a result of decay in tangential momentum. Vertical vorticity was also derived, and the highest values were found within the inner core region regardless of the elevation. From the vertical plane measurements, the smallest vertical velocities were found in the core centre, indicating deceleration of the upward motion. The highest vertical velocities were found at core edge, with magnitudes 60 - 70% of the

tangential components. In addition, the local swirl ratios around the core were calculated and found to have values greater than 1.0, suggesting a two-cell vortex structure within the measured height.

Acknowledgments

The authors acknowledge the financial support from the Marsden Grant (18-UOA-013), Royal Society of New Zealand.

References

Bischof, T., MacDonald, M., Cater, J. E., & Flay, R. G. J. (2020). Numerical Simulations of Laboratory–Scale Buoyancy Vortices. *22nd Australasian Fluid Mechanics Conference AFMC2020*, The University of Queensland.

Church, C. R., Snow, J. T., Baker, G. L., & Agee, E. M. (1979). Characteristics of Tornado-Like Vortices as a Function of Swirl Ratio: A Laboratory Investigation. *Journal of Atmospheric Sciences*, *36*(9), 1755-1776.

Fitzjarrald, D. E. (1973). A Field Investigation of Dust Devils. *Journal of Applied Meteorology and Climatology*, *12*(5), 808-813.

Golden, J. H. (1974a). The Life Cycle of Florida Keys' Waterspouts. I. *Journal of Applied Meteorology*, *13*(6), 676-692.

Golden, J. H. (1974b). Scale-Interaction Implications for the Waterspout Life Cycle. II. *Journal of Applied Meteorology*, *13*(6), 693-709.

Hawkes, N. A., Flay, R. G. J., Cater, E. J., & Macdonald, M. (2020). Scaling of Experimental Buoyancy Vortex Structures with Respect to Power Generation. Journal of Physics: Conference Series, Ser. vol. 1618, p. 032008.

Hess, G. D., & Spillane, K. T. (1990). Characteristics of Dust Devils in Australia. *Journal of Applied Meteorology*, *29*(6), 498-507.

Kuo, H. L. (1966). On the Dynamics of Convective Atmospheric Vortices. *Journal of the Atmospheric Sciences*, *23*(1), 25-42.

Lugt, H. J. (1989). Vortex Breakdown in Atmospheric Columnar Vortices. *Bulletin of the American Meteorological Society*, *70*(12), 1526-1537.

Mullen, J., & Maxworthy, T. (1977). A laboratory model of dust devil vortices. *Dynamics of Atmospheres and Oceans*, *1*, 181-214.

Rennó, N., Burkett, M., & Larkin, M. (1998). A Simple Thermodynamical Theory for Dust Devils. *Journal of The Atmospheric Sciences - J ATMOS SCI*, *55*, 3244-3252.

Renno, N. O., et al. (2004). MATADOR 2002: A pilot field experiment on convective plumes and dust devils. *Journal of Geophysical Research*, *109*(E7).

Simpson, M. W., & Glezer, A. (2016). Buoyancy-induced, columnar vortices. *Journal of Fluid Mechanics*, *804*, 712-748.

Sinclair, P. C. (1973). The Lower Structure of Dust Devils. *Journal of the Atmospheric Sciences*, *30*(8), 1599-1619.